Observation of Single Colloidal Platinum Nanocrystal Growth Trajectories

Haimei Zheng[1,2,3], Rachel K. Smith[3‡], Young-wook Jun[2,3‡], Christian Kisielowski[1,2], Ulrich Dahmen[1,2 #], A. Paul Alivisatos[2,3 *]

[1]*National Center for Electron Microcopy, Lawrence Berkeley National Laboratory, Berkeley, CA 94720, USA*

[2]*Materials Sciences Division, Lawrence Berkeley National Laboratory, Berkeley, CA 94720, USA*

[3]*Department of Chemistry, University of California, Berkeley, CA 94720, USA*

It is conventionally assumed that the growth of monodisperse colloidal nanocrystals requires a temporally discrete nucleation followed by monomer attachment onto the existing nuclei. However, recent studies have reported violations of this classical growth model, and have suggested that inter-particle interactions are also involved during the growth. Mechanisms of nanocrystal growth still remain controversial. Using *in situ* transmission electron microscopy, we show that platinum nanocrystals can grow either by monomer attachment from solution onto the existing particles or by coalescence between the particles. Surprisingly, an initially broad size distribution of the nanocrystals can spontaneously narrow. We suggest that nanocrystals take different pathways of growth based on their size- and morphology-dependent internal energies. These observations are expected to be highly relevant for other nanocrystal systems.

[‡]These authors contributed equally to this paper.
To whom correspondence should be addressed. [#]Email: udahmen@lbl.gov or [*]Email: alivis@berkeley.edu

The growth of colloidal nanocrystals has advanced remarkably in the last decade. Today it is possible to make colloidal nanocrystals of a wide range of solids, ranging from metals to semiconductors and insulators, with narrow size distributions (variation in diameter less than 5%) and high crystallinity (*1-5*). Further, it is also possible to control their shapes, from spheres to disks or rods, as well as their topology (solid, hollow, nested) and their connectivity and branching patterns (*6-11*). These advances in nanocrystal synthesis have enabled the creation of a new generation of nanomaterials which can be made as inexpensively as polymers, and which could be applied to as many technologies in the future as plastics are today. The current state of nanocrystal synthesis has been largely achieved empirically, with some classical models (*12-14*) for particle growth serving as guides. In this paper we demonstrate that it is possible to directly observe the growth trajectories of individual colloidal nanocrystals in solution using a newly designed liquid cell that operates inside a transmission electron microscope (TEM), and that these trajectories reveal a diverse set of pathways more complex than those envisioned previously.

To appreciate the potential value of single particle growth trajectories, consider the simplest case of a narrow size distribution of nearly spherical colloidal nanoparticles. A model based on kinetics that can account for this size distribution was first proposed by LaMer and Dinegar (*12*) and subsequently improved by Reiss (*13*). An abrupt increase in monomer concentration induces a burst of nucleation events, followed by a period of rapid growth. The initial broad size distribution due to a spread in nucleation time or due to other variations such as mixing can be corrected with “size distribution focusing”, in which small crystals “catch up” with larger ones because at relatively high monomer

concentration the growth rate of nanocrystals decreases as the size increases (*1*). Inhibition of particle aggregation is typically achieved by using surfactant ligands that stabilize the particle surface and provide a barrier to coalescence. The thinking underlying this approach has guided many syntheses (*1, 2, 4*). A second scenario for nanocrystal control employs an equilibrium approach. One devises a system where the binding of surfactant to the nanoparticle surface is nearly as strong as the bonds within the crystal, strong enough then to thermodynamically drive the system toward a particular average size for a given concentration of surfactant and monomeric species (*15-17*). These two clearly distinct models consider only the possibility of particle growth through the addition of monomeric species. However, there is substantial evidence that particle coalescence or even oriented attachment can also play a role in nanocrystal growth (*18-23*). The lack of consensus on the controlling mechanisms is mainly due to the lack of direct evidence for nanocrystal growth in solution. *In situ* observation of the dynamic growth process is expected to advance our understanding of nanocrystal growth mechanisms significantly.

In order to observe colloidal nanocrystal growth, one needs a technique that can image through liquids during the chemical reaction with nanometer resolution and in real time. Recently, Ross *et al.* have developed a liquid cell reactor that can be placed in a special TEM sample holder, which was used to image the dynamic growth of Cu clusters on a surface during electrochemical plating using a TEM with a resolution of 5 nm (*24*) (also see other related techniques (*25, 26*)). Here, we employ this TEM capability in a newly designed self-contained liquid cell with an improved resolution in the sub-nanometer range (see the details on the liquid cells in SOM). These disposable liquid

cells have been used to image platinum nanocrystal growth in solution *in situ* using a JEOL3010 microscope operated at 300 kV. Since the cells fit into a standard TEM sample holder, CM300 and CM200 TEMs equipped with an x-ray detector were also used for high resolution TEM imaging and elemental analysis *ex situ* on the same cell. A stock solution for synthesis was prepared by dissolving Pt(acetylacetonate)$_2$ (10 mg/mL) in a mixture of *o*-dichlorobenzene and oleylamine (9:1 in volume ratio). About 100 nanoliters of the growth solution was loaded into the reservoir of a liquid cell and the solution was drawn into the cell by capillary force. Subsequently, the cell was sealed and loaded into the microscope. Within the electron transparent window, the reaction solution of about 200 nm in thickness was confined between two silicon nitride membranes (25 nm each).

A key feature of the present experiment is the ability to use the electron beam to induce the nucleation of the Pt nanocrystals. When the electron beam is focused to a current density of 2-14x10^4 A/m^2, the growth of Pt nanocrystals in solution is initiated (*27*). A constant beam intensity is maintained during the growth. However, the intensity does vary briefly in the initial exposure to the electron beam during the time period required to focus for imaging (a few seconds). Some nanoparticles nucleate during this period. Subsequently, under constant illumination, there is a new round of nucleation followed by the growth. It is remarkable that high quality platinum nanocrystals are formed. Fig. 1A shows platinum nanocrystals obtained inside a liquid cell by exposure of the growth solution to the electron beam for about 5 min. Nearly monodisperse nanoparticles with an average diameter of 3.5 nm (± 0.3 nm) are obtained (Fig. 1A inset). The nanoparticles are mostly single crystalline with a face centered cubic structure (see

Fig. 1B) and a composition of pure Pt, as confirmed by Energy Dispersive X-ray Spectroscopy (EDS) (Fig. 1C).

In situ observation of the Pt nanoparticle growth provides details of the growth kinetics. Fig. 2 shows a sequence of video images recorded at 0 s, 12.07 s, 24.23 s and 77.00 s of exposure to electron beam radiation (also see Mov. S1). From the initial growth solution of Pt^{2+} precursor, a large number of Pt nanocrystals emerge and new particles continue to appear, spanning an interval of more than 10 seconds. Particle growth and nucleation occur in parallel (see particles highlighted by arrows in Fig. 2A indicating examples of growth). Interestingly, along with the conventional particle growth by monomer addition from solution, frequent coalescence events between the particles are observed. At the early stage of the growth, the number of particles gradually increases and reaches a maximum at 21 seconds. Subsequently, the number of particles drops significantly and eventually settles at a constant value. Although some smaller particles are seen to dissolve completely, the decrease in the number of particles is mainly due to the coalescence events between individual particles (see the number of coalescence events as a function of time in Fig. 2B).

Particles that are of similar initial size but evolve along different pathways, through simple growth (*e.g.* monomer addition) or coalescence, are closely examined. Fig. 3A shows a sequence of video frames of two such particles, which were taken from the same field of view (also see Fig. S2). Similar final particle sizes are observed although the two particles arose through distinctly different paths. The particle formed by simple growth shows a continuous increase of size and maintains nearly spherical shape. In addition, mostly uniform diffraction contrast within the particle is observed indicating

single crystalline characteristics throughout the growth. However, the coalesced particle shows both shape changes and different diffraction contrast indicating polycrystalline characteristics within the particle after the coalescence event. Eventually (about 16 s after the coalescence event) it forms a single crystalline particle with nearly spherical shape. This is characteristic of punctuated growth, where the combined particles due to coalescence events eventually, after a pause in growth (relaxation), catch up with particles that are formed by simple growth.

We have also analyzed the effects of coalescence and punctuated growth on the particle size distribution. Until now, most nanocrystal growth models predict focusing of particle size via attachment of monomeric species and an Ostwald ripening process but have overlooked the effect of coalescence. Intuitively, it seems that coalescence should result in a broad size distribution and thus should be avoided. Our results from a large number of experiments suggest otherwise. Fig. 4A shows the histograms of particle size distribution at different stages of growth (19.7 s, 24.2 s, 30.3 s and 77 s; for each plot, about 120-170 particles within an area of 50 nm x 60 nm and during 10 milliseconds of growth were measured). At the early stages, particle size distributions are broad. At 24.2 s, we observe a bimodal distribution, which is mainly due to a large number of coalescence events. These early-stage size distributions behave exactly as expected, but at a later stage, the initially broad distribution spontaneously narrows.

In order to understand this unexpected size-focusing behavior, we have examined the growth trajectories of each individual nanoparticle. Fig. 4B shows particle size as a function of growth time for a few selected particles as examples (particles are highlighted by arrows in Fig. 2A), in which an effective size of $d = 2 \cdot \sqrt{A/\pi}$ was used, where A is the

two-dimensional area of the particle in the video images. A particle evolving by simple growth shows a continuous increase of size until it reaches a saturation stage (particle 1). However, particles resulting from coalescence events (particles 2, 3, 4 and 5) show a jump of particle size after each coalescence event. A smaller particle can "catch up" to the size of a bigger particle by multiple coalescence events. The fact that multiple coalescence events are more commonly observed among the small particles is attributed to their higher energy due to a larger surface to volume ratio and an increased collision frequency resulting from a greater mobility. Such growth kinetics of individual nanoparticles deviates from the behavior of ensemble, shown in Fig. 4C, which reflects the average particle size within an area of 50 nm x 60 nm as a function of time. Interestingly, in spite of the diverse trajectories of growth, the growth kinetics of ensemble can be described by a diffusion controlled Ostwald ripening process (the size of the particles (d) is proportional to growth time (t), $d^3 \sim t$) followed by saturation (Fig. 4C), which resembles the trend predicted by classical growth models (*2*). In perhaps the most remarkable and unexpected observation associated with these experiments, we find that there is a period of time after a coalescence event, during which the coalesced particles cease to grow. After the relaxation, the particle resumes growth through monomer addition. The combined effects of monomer addition, coalescence and punctuated growth, all contribute to the focusing of the size distribution.

It is interesting to consider the origin of the pause in growth just after a coalescence event. During coalescence the combined particle has higher internal energy and chemical potential because of the appearance of grain boundaries and higher surface energy determined by its shape compared with a spherical particle of the same size. Such

higher energy particles may lose monomers (dissolve) in the solution and/or change shape. Similar effects have been observed in the growth of Ge islands from a vapor phase (*28*). In our case, the combined nanoparticle changes shape forming a spherical particle. During the relaxation, along with the recrystallization a slight decrease of particle size has been observed in some cases (*e.g.* Fig. 4B). We further found that the relaxation time (τ, highlighted in Fig. 4B inset) increases with the particle size (d) following a power law relationship, $\tau \sim d^{3.3}$ (Fig. 4D). When considering the relaxation process as a recrystallization process where monomeric species migrate on the two-dimensional nanocrystal surface, such a result is fairly reasonable. The relaxation time is proportional to the total surface area ($A = \frac{1}{4}\pi \cdot d^2$) and inversely proportional to the mobility (β) of monomers on the particle surface, $\beta \propto \frac{1}{d}$, where *1/d* is the curvature of the particle. Therefore, the relationship between the relaxation time and the size of the coalesced particles is estimated by $\tau \sim d^3$, which is close to our experimentally observed value. However, this is only a rough estimation, additional factors such as variations in the nature of coalescence (oriented or random attachment), details of size and shape of the coalesced particle need to be considered for more accurate evaluation (*29*).

Additionally, we found that oleylamine surfactants play a significant role in particle size focusing. In nanocrystal synthesis, it is considered that particles stop growth when the system achieves an equilibrium state that the monomer in solution is balanced with the solubility of the nanocrystals. Such an equilibrium state is modified by surfactants, for example, surfactants with a close-packed configuration on a particle surface can effectively stop the particle growth at a certain size (*15*). In order to examine

the surfactant effects, we decreased the amount of oleylamine in the growth solution (0-3%) for comparison. The fact that platinum crystal foils and dendrites are observed in those cases (Fig. S3) confirms that the surfactants play a critical role in the growth of monodisperse platinum nanocrystals.

In summary, we have observed the dynamic growth of colloidal platinum nanocrystals in solution with sub-nanometer resolution using a TEM. The evolution of monodisperse platinum nanocrystals involves complex growth trajectories and significant coalescence events, features that have not been considered in the classical models for nanocrystal growth. Considering coalescence as an alternative to simple growth by attachment of monomeric species, we expect that growth by particle attachment may also play an important role in the synthesis of nanocrystals with more complex shapes. More generally, we have shown that *in situ* TEM enables visualization of single nanoparticles in solution with sub-nanometer resolution and offers great potential for addressing many fundamental issues in materials science, chemistry and other fields of science.

References and Notes

1. X. G. Peng, J. Wickham, A. P. Alivisatos, *J. Am. Chem. Soc.* **120**, 5343 (1998).
2. C. B. Murray, C. R. Kagan, M. G. Bawendi, *Annu. Rev. Mater. Sci.* **30**, 545 (2000).
3. B. L. Cushing, V. L. Kolesnichenko, C. J. O'Connor, *Chem. Rev.* **104**, 3893 (2004).
4. Y. Yin, A. P. Alivisatos, *Nature* **437**, 664 (2005).
5. D. J. Norris, A. L. Efros, S. C. Erwin, *Science* **319**, 1776 (2008).
6. X. G. Peng *et al.*, *Nature* **404**, 59 (2000).
7. L. Manna, E. C. Scher, A. P. Alivisatos, *J. Am. Chem. Soc.* **122**, 12700 (2000).
8. V. F. Puntes, K. M. Krishnan, A. P. Alivisatos, *Science* **291**, 2115 (2001).
9. V. F. Puntes, D. Zanchet, C. K. Erdonmez, A. P. Alivisatos, *J. Am. Chem. Soc.* **124**, 12874 (2002).
10. D. J. Milliron *et al.*, *Nature* **430**, 190 (2004).
11. Y. D. Yin *et al.*, *Science* **304**, 711 (2004).
12. V. K. LaMer, R. H. Dinergar, *J. Am. Chem. Soc.* **72**, 4847 (1950).
13. H. Reiss, *J. Chem. Phys.* **19**, 482 (1951).
14. T. Sugimoto, *Adv. colloid Interface Sci.* **28**, 65 (1987).
15. D. V. Leff, P. C. Ohara, J. R. Heath, W. M. Gelbart, *J. Phys. Chem. B* **99**, 7036 (1995).
16. Y. Chen, E. Johnson, X. Peng, *J. Am. Chem. Soc.* **129**, 10937 (2007).
17. Y. A. Yang, H. M. Wu, K. R. Williams, Y. C. Cao, *Angew. Chem. Int. Ed.* **44**, 6712 (2005).

18. R. L. Penn, J. F. Banfield, *Geochim. Cosmochim. Acta* **63**, 1549 (1999).

19. J. F. Banfield, S. A. Welch, H. Z. Zhang, T. T. Ebert, R. L. Penn, *Science* **289**, 751 (2000).

20. C. Pacholski, A. Kornowski, H. Weller, *Angew. Chem. Int. Ed.* **41**, 1188 (2002).

21. J. H. Yu *et al.*, *J. Am. Chem. Soc.* **127**, 5662 (2005).

22. J. Zhang *et al.*, *J. Am. Chem. Soc.* **128**, 12981 (2006).

23. M. Niederberger, H. Colfen, *Phys. Chem. Chem. Phys.* **8**, 3217 (2006).

24. M. J. Williamson, R. M. Tromp, P. M. Vereecken, R. Hull, F. M. Ross, *Nature Mater.* **2**, 532 (2003).

25. P. L. Gai, *Microsc. Microanal.* **8**, 21 (2002).

26. K. L. Liu *et al.*, *Lab Chip* **8**, 1915 (2008).

27. See Supporting Online Material.

28. F. M. Ross, J. Tersoff, R. M. Tromp, *Phys. Rev. Lett.* **80**, 984 (1998).

29. J. E. Burke, D. Turnbull, *Progress in Metal Physics, Pergamon Press, London* **3**, 220 (1952).

30. The authors would like to thank Dr. A. Minor for the helpful discussions on the liquid cells. This project is supported by Helios SERC founded by the Director, Office of Science, Office of Basic Energy Sciences, Materials Sciences and Engineering Division of the U.S. Department of Energy under Contract No. DE-AC02-05CH11231.

Supporting Online Material

www.sciencemag.org

Materials and Methods

Figs. S1, S2, S3

Movie S1

References

Figure Captions:

Fig. 1. TEM analysis of Pt nanocrystals synthesized in a liquid cell. **A.** Bright field TEM image of Pt nanocrystals with inset histogram of particle size distribution, obtained from measurements of 150 particles. **B.** High resolution TEM image of a Pt nanocrystal, which was recorded after the *in situ* experiment. **C.** EDS spectra from Pt nanocrystals (red) and background (black) obtained *ex situ* from the same liquid cell. The observed Si and Cu signals are from the silicon nitride membrane window and the cover of the liquid cell, respectively.

Fig. 2. Growth and coalescence of Pt nanocrystals. **A.** Video images acquired at 0 s, 12.07 s, 24.23 s and 77 s of exposure to the electron beam during the growth of Pt nanocrystals. Specific particles are labeled by arrows. The growth trajectories of these individual particles reveal the diverse pathways leading to size focusing. **B.** Number of particles (left axis) and number of coalescence events (Nc, right axis) during an interval of 2 s *vs* time. Particles nucleate and grow during the adjustment of focus for imaging (0-10 s), the details of which were not available.

Fig. 3. Comparison of different growth trajectories. **A.** Video images showing simple growth by monomer addition (left column) or growth by coalescence (right column). Particles are selected from the same field of view. **B.** Enlarged (1.5 times) color images of (A). Distinct contrast changes indicating recrystallization are observed in the coalesced particle but not in the case of simple growth. Contrast differences within the particle are highlighted by arrows.

Fig. 4. Growth kinetics of Pt nanoparticles. **A.** Histograms of particle size distribution at 19.7 s, 24.2 s, 30.3 s and 77 s, respectively. Black curves are Gaussian fits. **B.** Particle

size *vs* growth time. Error bars for particle diameter measurements are ± 0.2 nm. These particles are highlighted in Fig. 2A. Inset shows two types of growth trajectories. A relaxation time (τ) was observed after a coalescence event. **C.** Logarithmic relationship of particle size *vs* growth time for the ensemble and those individual particles 1-5 in (B). Black lines are guides to eye and dashed lines show the coalescence events. **D.** Logarithmic relationship of relaxation time *vs* the size of the coalesced particles. Black line shows linear fit.

Fig. 1.

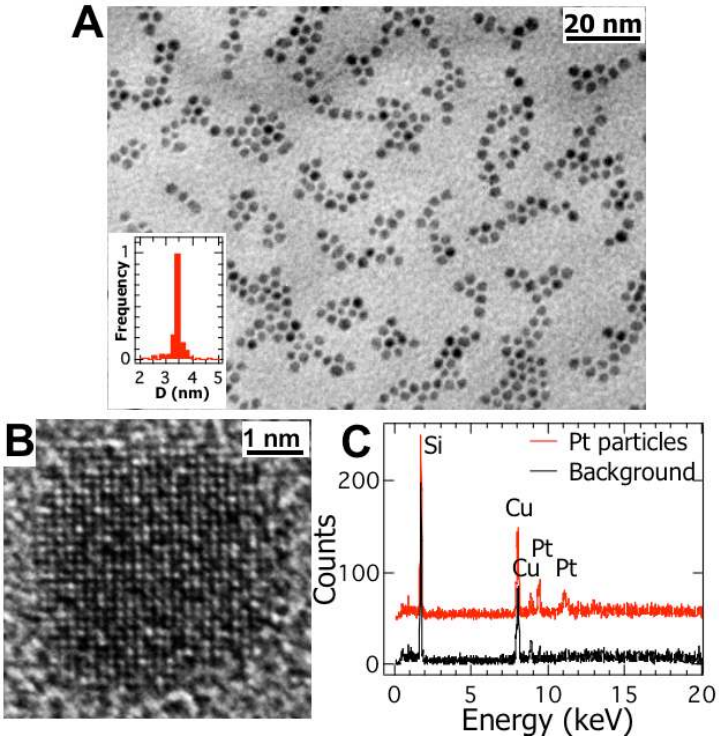
A
20 nm
Frequency
1
0
2 3 4 5
D (nm)
B
1 nm
C
Si
Pt particles
Background
200
100
0
Counts
Cu
Pt
Cu
Pt
0 5 10 15 20
Energy (keV)

Fig. 2.

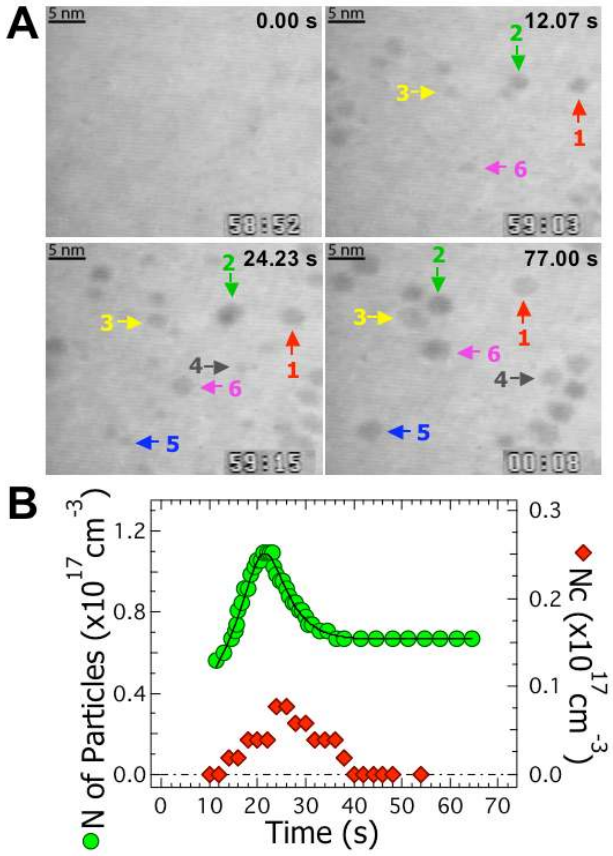
A
5 nm
0.00 s
58:52
12.07 s
59:03
24.23 s
59:15
77.00 s
00:08
1
2
3
4
5
6
B
N of Particles (x10^17 cm^-3)
Nc (x10^17 cm^-3)
Time (s)
0.0
0.4
0.8
1.2
0.1
0.2
0.3
0
10
20
30
40
50
60
70

Fig. 3.

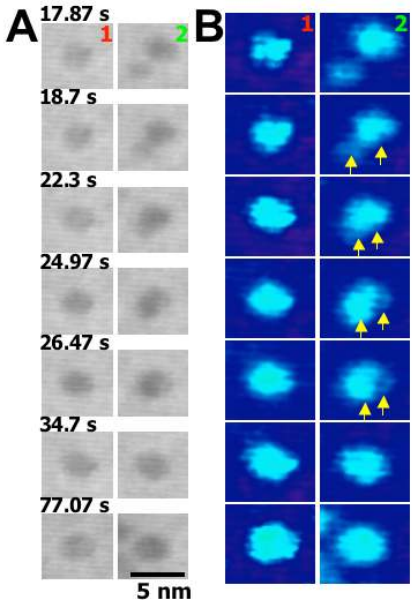

Fig. 4.

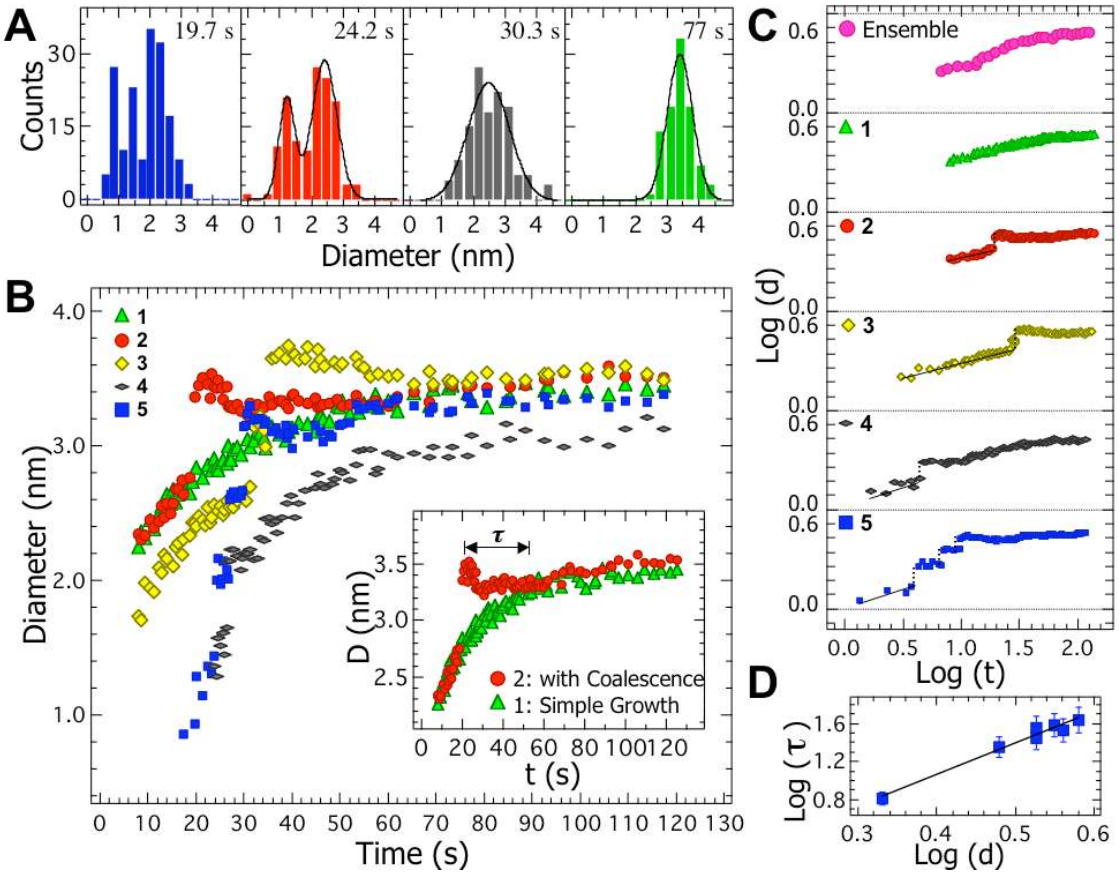
A
19.7 s
24.2 s
30.3 s
77 s
Counts
Diameter (nm)
B
Diameter (nm)
Time (s)
1
2
3
4
5
D (nm)
t (s)
τ
2: with Coalescence
1: Simple Growth
C
Ensemble
Log (d)
Log (t)
D
Log (τ)
Log (d)

Supporting Online Material

for

Observation of Single Colloidal Platinum Nanocrystal Growth Trajectories

Haimei Zheng[1,2,3], Rachel K. Smith[3 ‡], Young-wook Jun[2,3 ‡], Christian Kisielowski[1,2], Ulrich Dahmen[1,2 #], A. Paul Alivisatos[2,3 *]

To whom correspondence should be addressed. [#]Email: udahmen@lbl.gov or [*]E-mail: alivis@berkeley.edu

[‡]These authors contributed equally to this paper.

This file includes:

I. Materials and Methods

All chemicals including Pt(acetylacetonate)$_2$ (99%, Aldrich), *o*-dichlorobenzene (99%, Aldrich) and oleylamine (70%, Aldrich) were used as received.

Liquid cell fabrication and growth solution loading for TEM A schematic of the liquid cell design is shown in Fig. S1. Cells were fabricated using ultra thin silicon wafers (100 μm, 4-inches, p-doped) purchased from Virginia Semiconductor (Fredericksburg, VA). The fabrication process includes vapor growth of low stress silicon nitride membranes on the silicon wafers (25 nm in thickness) followed by lithographic patterning, etching and bonding. The bottom and top pieces of the liquid cell were bonded together at 120 °C for 1h using a thin layer of indium. The indium layer was deposited on the bottom piece by following the process of lithographic patterning, indium deposition by sputtering, and lift-off. Indium acts as a spacer as well as the sealing material for the liquid cell. 200 nm indium spacing was used for the current experiments, although different thickness can be achieved. All the fabrication processes were conducted at the Microfabrication Lab of the University of California at Berkeley.

About 100 nL of liquid is loaded into the cell. The liquid loading is facilitated by a syringe and Teflon nanotube (purchased from Cole-Parmer, VH, IL) to control the liquid droplet size and a micromanipulator to precisely direct the droplets in the liquid reservoir without contaminating the electron transmission window.

Initiation of the growth of platinum nanocrystals The growth of Pt nanocrystals in solution is initiated by focusing of the electron beam to a current density of 2-14 × 10^4 A/m^2 on the precursor solution. The reduction of Pt(acetylacetonate)$_2$ precursor (Pt^{2+}) to platinum metal (Pt^0) can be from either I) oleylamine-assisted metal ion reduction at an elevated temperature (scheme I), or II) reduction by the solvated free-electrons from inelastic scattering of the incident electron beam (scheme II) (1-5).

$$Pt^{2+} + 2RNH_2 \xrightarrow{\Delta} Pt^0 + 2RNH_2^+ \quad \text{(scheme I)}$$

$$Pt^{2+} + 2e^- \xrightarrow{\Delta} Pt^0 \quad \text{(scheme II)}$$

Since our experiments show that formation of platinum nanocrystals in flasks occurs only above 180 °C using the same growth solution but the local temperature rise in a liquid cell due to electron beam heating should be less than a few degrees (6), the reduction of platinum ions is probably mainly by the solvated electrons (scheme II).

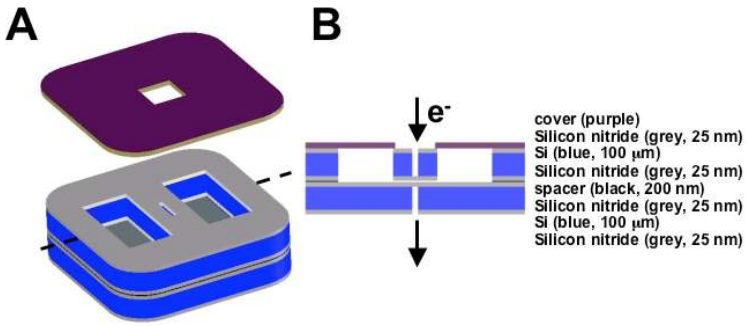

Fig. S1. A liquid cell schematic. (**A**) Three-dimensional view. Lateral dimensions of the liquid cell: 2.6×2.6 mm and 3 mm in diagonal; reservoirs: 0.6×1.2×0.1 mm; the electron transparent window: 1×50 μm; cover: 0.6×0.6 mm for the hole and its outer dimensions are the same as the liquid cell. (**B**) Cross-sectional view of the plane marked in (A).

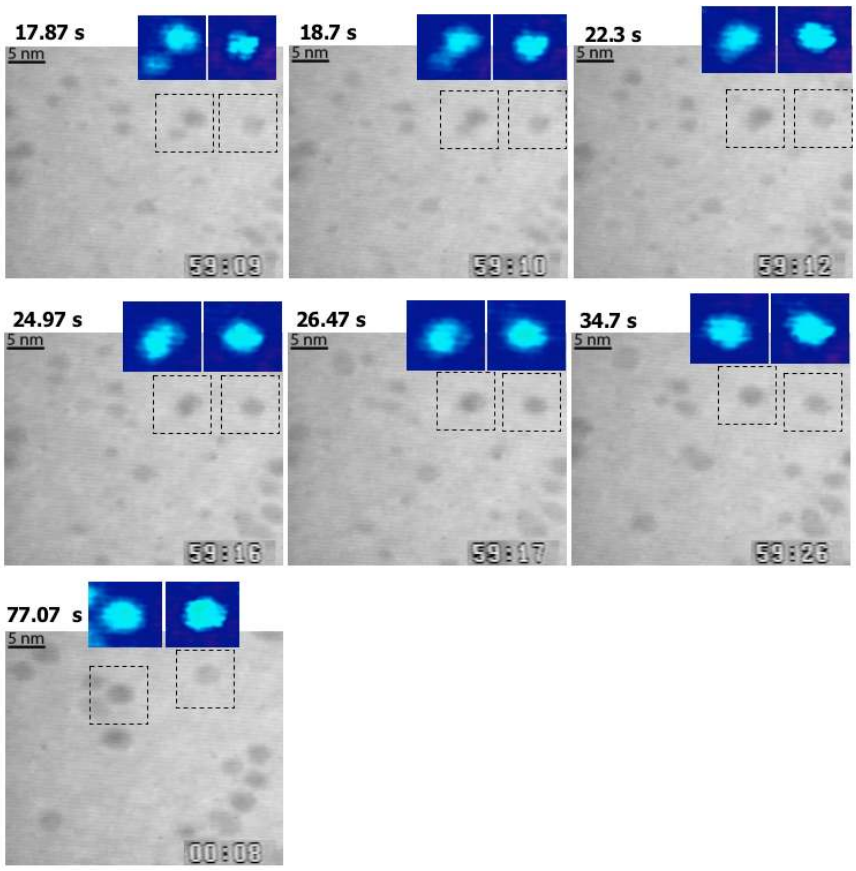

Fig. S2. Comparison of different growth trajectories. The selected particles with the enlarged (1.5 times) color images show two types of growth, either by simple growth of monomer attachment or coalescence. Distinct contrast changes indicating recrystallization are observed in the coalesced particle but not in the case of simple growth.

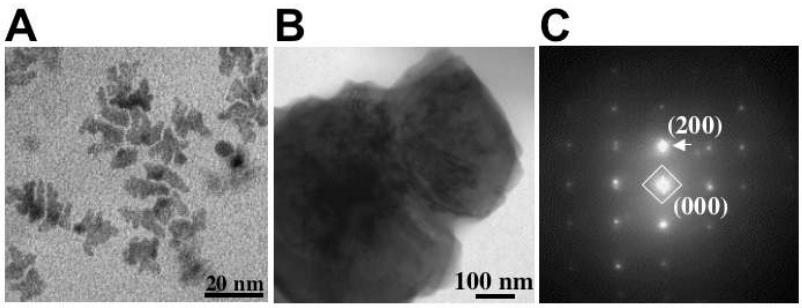

Fig. S3. Formation of platinum dendrites and "foil" when the volume fraction of oleylamine was decreased (0-3%) in the growth solution. **A.** Platinum dendrites. **B.** Platinum "foil" was observed in some cases when no oleylamine surfactant was used. **C.** Selected area diffraction from (B) showing platinum "foil" is crystalline with a face centered cubic structure.

References

1. M. Aslam, L. Fu, M. Su, K. Vijayamohanan, V. P. Dravid, *J. Mater. Chem.* **14**, 1795 (2004).
2. J. D. S. Newman, G. J. Blanchard, *Langmuir* **22**, 5882 (2006).
3. C. K. Harnett, K. M. Satyalakshmi, H. G. Craighead, *Appl. Phys. Lett.* **76**, 2466 (2000).
4. D. F. Silva, A. O. Neto, E. S. Pino, *Mater. Res.* **10**, 367 (2007).
5. S. Seino *et al. J. Nanopart. Res.* **10**, 1071 (2008).
6. R. F. Egerton, P. Li, M. Malac, *Micron* **35,** 399 (2004).

Movie Caption

Movie S1: Growth of platinum nanocrystals in a liquid cell observed *in situ* using a TEM. Time is labeled in the format of minute : second.